Electronic Supplementary Material (ESI) for Journal of Materials Chemistry C.

Au Nanorod Plasmonic Superstructures Obtained by a Combined Droplet Evaporation and Stamping Method

Carola Schopf, Alfonso Martín, Mícheál Burke, Daniel Jones, Andrea Pescaglini, Alan O'Riordan, Aidan J. Quinn and Daniela Iacopino

Supporting Information

Au nanorod synthesis.

Seed Solution (Nanorods 14 × 44 nm (AR = 3.1), 11 × 40 nm (AR =3.6, 10 × 41 nm (AR = 4.1)

CTAB solution (3.75 mL, 0.15 M) was mixed with 1.25 mL of 1 mM $HAuCl_4$. To the stirred solution 0.3 mL of ice-cold 0.01 M $NaBH_4$ was added under vigorous stirring, which resulted in the formation of a pale brown solution. Vigorous stirring of the seed solution was continued for 2 min. Solution was kept at 30 °C until further use.

Seed Solution (Nanorods 23 × 49 nm, AR = 2.1)

CTAB solution (3.75 mL, 0.15 M) was mixed with 1.25 mL of 1 mM $HAuCl_4$. To the stirred solution 0.3 mL of ice-cold 6.5 mM $NaBH_4$ was added under vigorous stirring, which resulted in the formation of a pale brown solution. Vigorous stirring of the seed solution was continued for 2 min. Solution was kept at 30 °C until further use.

Growth of Nanorods (11 × 40 nm, 23 × 49 nm)

CTAB (12.5 mL, 0.15 M) was added to 0.5 mL of 4 mM of $AgNO_3$ at 30 °C. To this solution, 12.5 mL of 1 mM $HAuCl_4$ was added, and after gentle mixing of the solution 0.18 mL of 0.0788 M ascorbic acid was added. Upon addition of ascorbic acid the solution color changed from intense orange to colorless. Finally, 35 μL of seed solution were added at 30 °C. The color of the solution gradually changed from colorless to intense red (10-20 min). The solution was stirred at 30 °C until growth process was complete (90-120 min) as indicated by further absence of spectral changes in the solution UV-Vis spectrum.

Growth of Nanorods (14 × 44 nm)

CTAB (12.5 mL, 0.15 M) was added to 1 mL of 4 mM of $AgNO_3$ at 30 °C. To this solution, 25 mL of 1 mM $HAuCl_4$ was added, and after gentle mixing of the solution 0.35 mL of 0.0788 M ascorbic acid was added. Upon addition of ascorbic acid the solution color changed from intense orange to colorless. Finally, 35 μL of seed solution were added at 30 °C. The color of the solution gradually changed from colorless to intense red (10-20 min). The solution was stirred at 30 °C until growth process was complete (90-120 min) as indicated by further absence of spectral changes in the solution UV-Vis spectrum.

Growth of Nanorods (10 × 41 nm)

CTAB (12.5 mL, 0.15 M) was added to 1 mL of 4 mM of $AgNO_3$ at 30 °C. To this solution, 12.5 mL of 1 mM $HAuCl_4$ was added, and after gentle mixing of the solution 0.18 mL of 0.0788 M ascorbic acid was added. Upon addition of ascorbic acid the solution color changed from intense orange to colorless. Finally, 35 μL of seed solution were added at 30 °C. The color of the solution gradually changed from colorless to intense red (10-20 min). The solution was stirred at 30 °C until growth process was

complete (90-120 min) as indicated by further absence of spectral changes in the solution UV-Vis spectrum.

Organic solvent transfer

Au nanorods in water solution were centrifuged and redispersed in water so that the final CTAB concentration was lower than 0.05 mM. Mercaptosuccinic acid (3 mL, 10 mM) was added to 3 mL of aqueous nanorod solution. The pH was adjusted to 9 under vigorous stirring. To this solution 1.5 mL of a 50 mM solution of TOAB in chlorobenzene was added. The resulting mixture was left under vigorous stirring for 30 min until the water phase discolored and the organic phase became intense red.

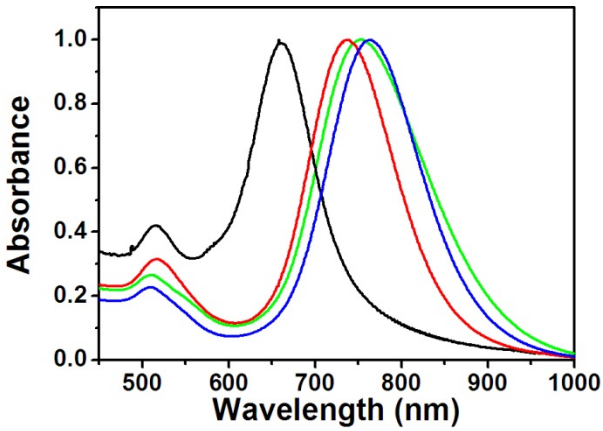

Figure SI1. UV-vis spectra of synthesized nanorods dispersed in water; 23×49 nm, AR = 2.1, black curve; 14×44 nm, AR = 3.1, red curve; 11×40 nm, AR = 3.6 nm, green curve; 10×41 nm, AR = 4.1, blue curve.

Effect of nanorod concentration

Assemblies formed across a relatively large range of Au nanorod concentrations, ranging from 0.1 nM to 10 nM. Figure SI2 shows different magnification SEM images of superstructures formed from evaporation of 0.5, 2 and 10 nM nanorod solutions. Droplet deposition of low concentration nanorod solutions was useful to elucidate the mechanism of superstructure formation. Nanorods assembled in parallel configurations within domains of sizes ranging from 0.5 to 200 μm^2, depending on the initial concentration of nanorods in the droplet. At high nanorod concentrations separation between domains decreased until, for nanorod concentrations of 10 nM and higher, domains merged and covered the entire area of a 5 mm diameter drop.

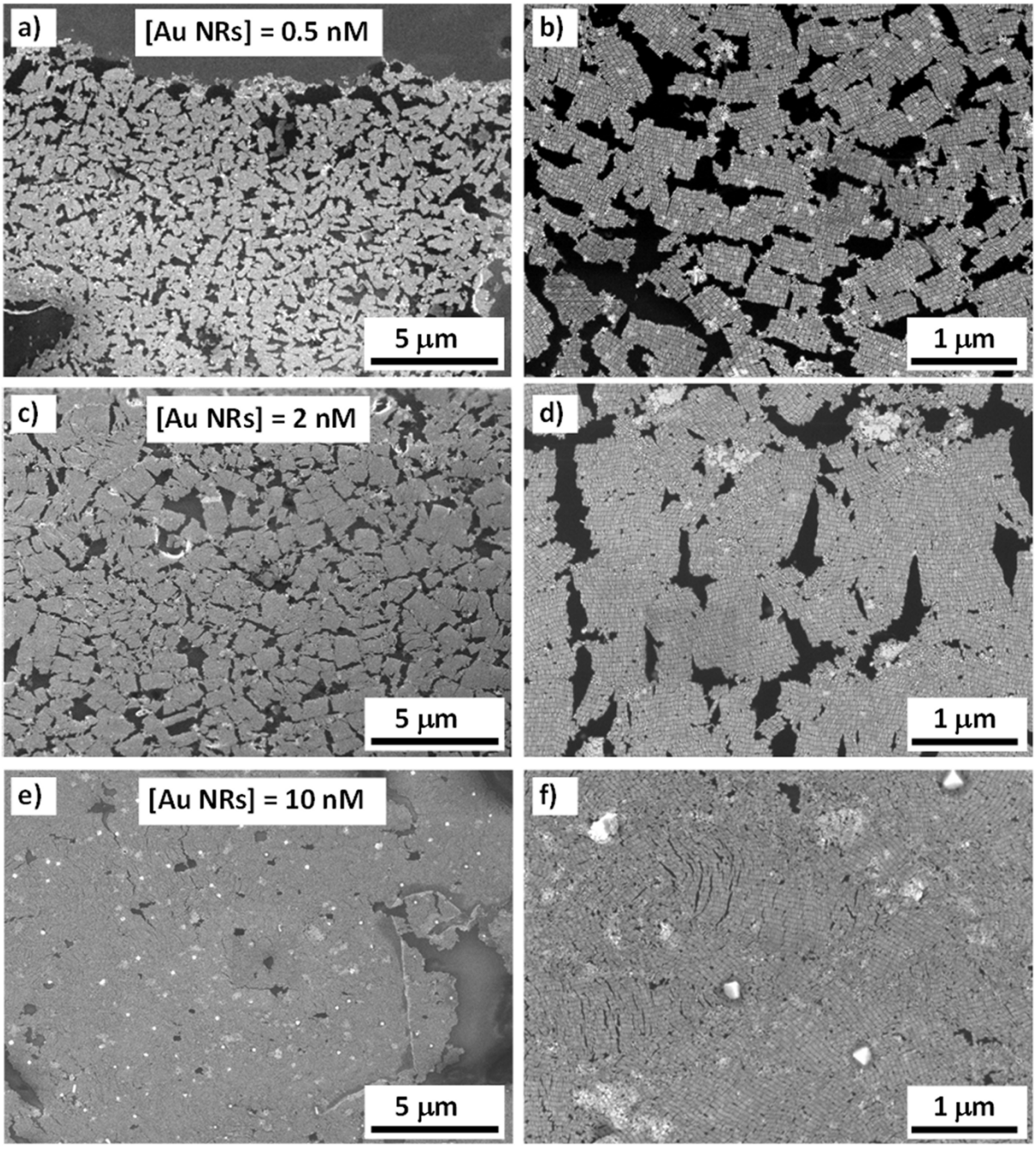

Figure SI2. Low (a, c, e) and high (b, d, f) magnification SEM images of parallel Au nanorod (AR = 3.6) superstructures obtained from evaporation of solutions with concentrations of 0.5 mM, 2 nM and 10 nM. Images show progressive increase of domain size accompanied by progressive coverage of the entire area of the 5 mm diameter deposited drop.

Effect of surfactant concentration

Ordered assemblies formed when CTAB concentration was kept between 0.01 and 0.2 mM. Higher CTAB concentrations led to disordered assemblies (see Figure SI3). At lower CTAB concentration nanorods did not transfer into chlorobenzene.

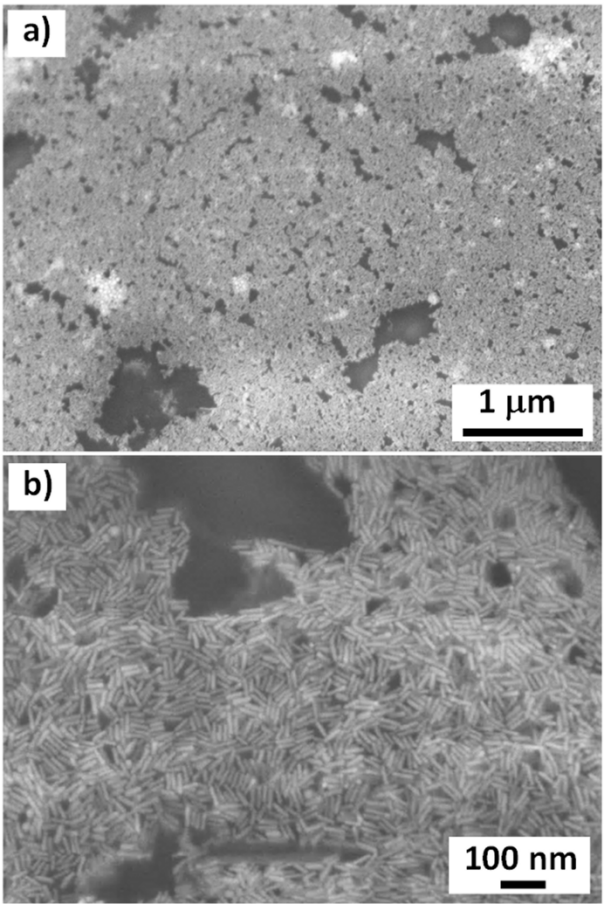

Figure SI3. a) Low and b) high magnification SEM image of assemblies formed by droplet deposition of nanorods (AR = 3.6) with CTAB concentration of 0.6 mM.

Effect of evaporation rate

The evaporation rate had a significant influence on the formation of ordered superstructures. Best results were obtained at room temperature when the evaporation time was slowed down to ca. 3h by covering the droplet with a petri dish. When no control of the evaporation rate was applied, disordered assemblies of nanorods were formed, as solvent evaporation was too fast for Au nanorods to organize into superstructures. Figure SI4a-b shows SEM images of assemblies formed upon deposition of chlorobenzene solutions on SiO_2 substrates. The evaporation rate was less than 1 h, as the droplet was not covered with a petri dish. As result poor degree of order was obtained.

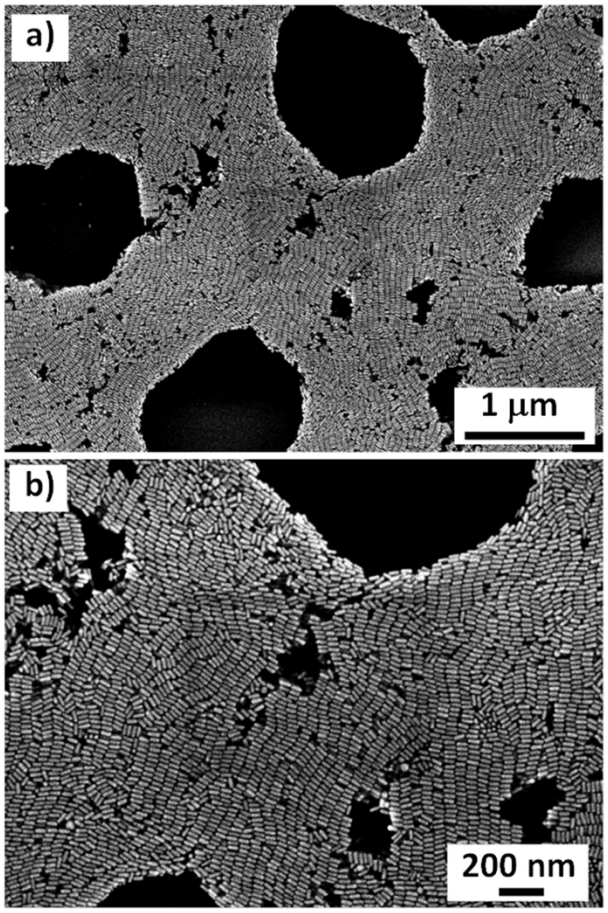

Figure SI4. A) Low and b) high magnification SEM images of Au nanorod (AR= 3.6) assemblies formed by fast droplet evaporation in air (no petri dish). Nanorods assembled in domains of 100 nm diameter average size.

Effect of aspect ratio

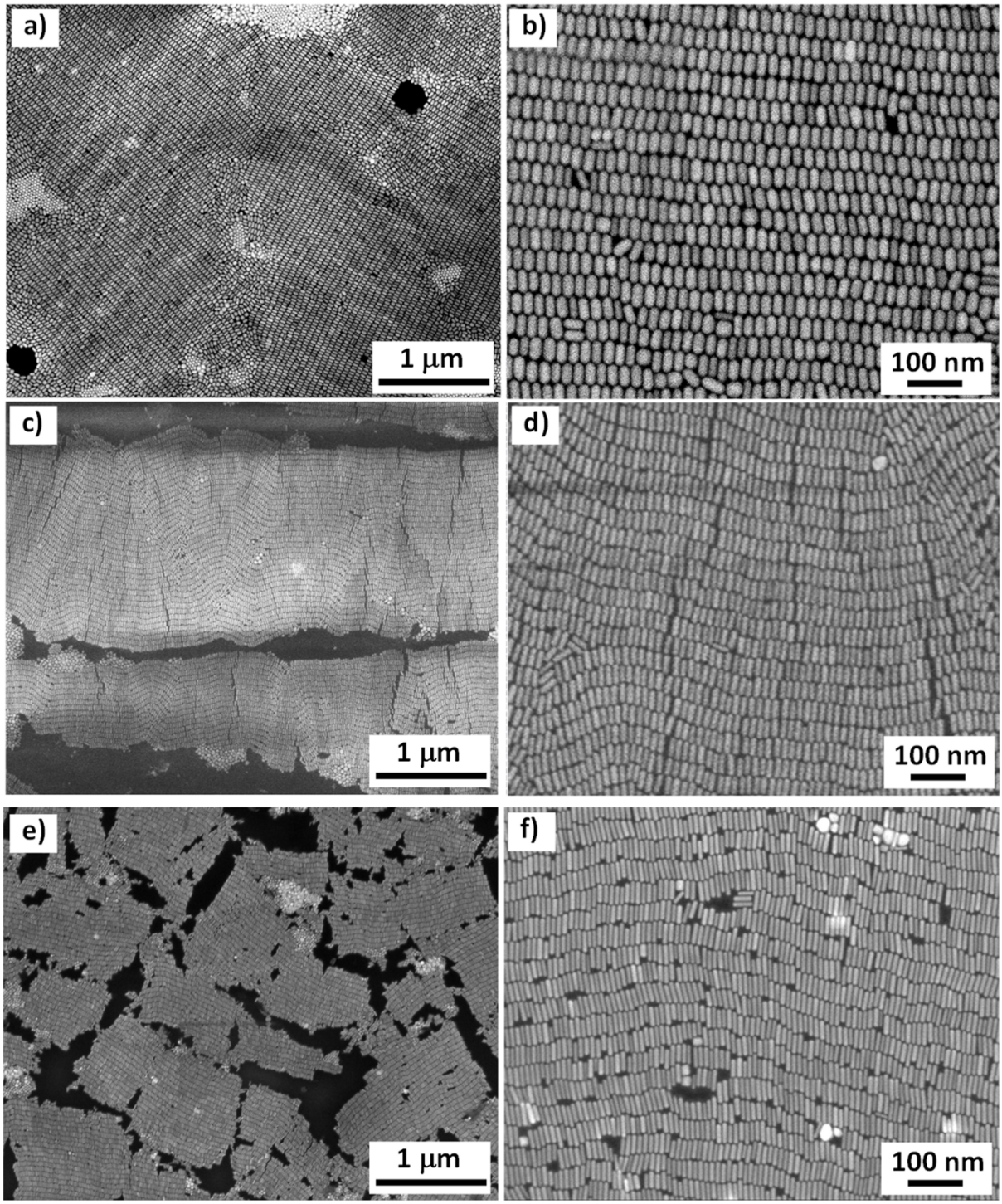

Figure SI5. Low and high magnification SEM images of parallel superstructures obtained from Au nanorods drop-deposited on SiO_2. Nanorod AR = 2.1 (a, b), 3.1 (c,d) and 4.1 (e, f).

Large areas of ordered monolayer superstructures with nanorods assembled side-by-side to form 2D monolayers were obtained from nanorods with aspect ratios between 2 and 4. Aspect ratios higher than 4 could not be investigated as these nanorods did not transfer from aqueous to organic phase. Figure SI5 shows low and high magnification SEM images of parallel superstructures formed by deposition of 10 μl, 10 nM chlorobenzene solutions of Au nanorods with the following characteristics: a) mean diameter 49 ± 3 nm, mean length 23 ± 2 nm, AR = 2.1, SPR= 690 nm, c) mean diameter 44 ± 2 nm, mean length 14 ± 2 nm, AR = 3.1, SPR= 720 nm; e) mean diameter 41 ± 3 nm, mean length 10 ± 2 nm, AR = 4.1, SPR= 792 nm.

Effect of solvent

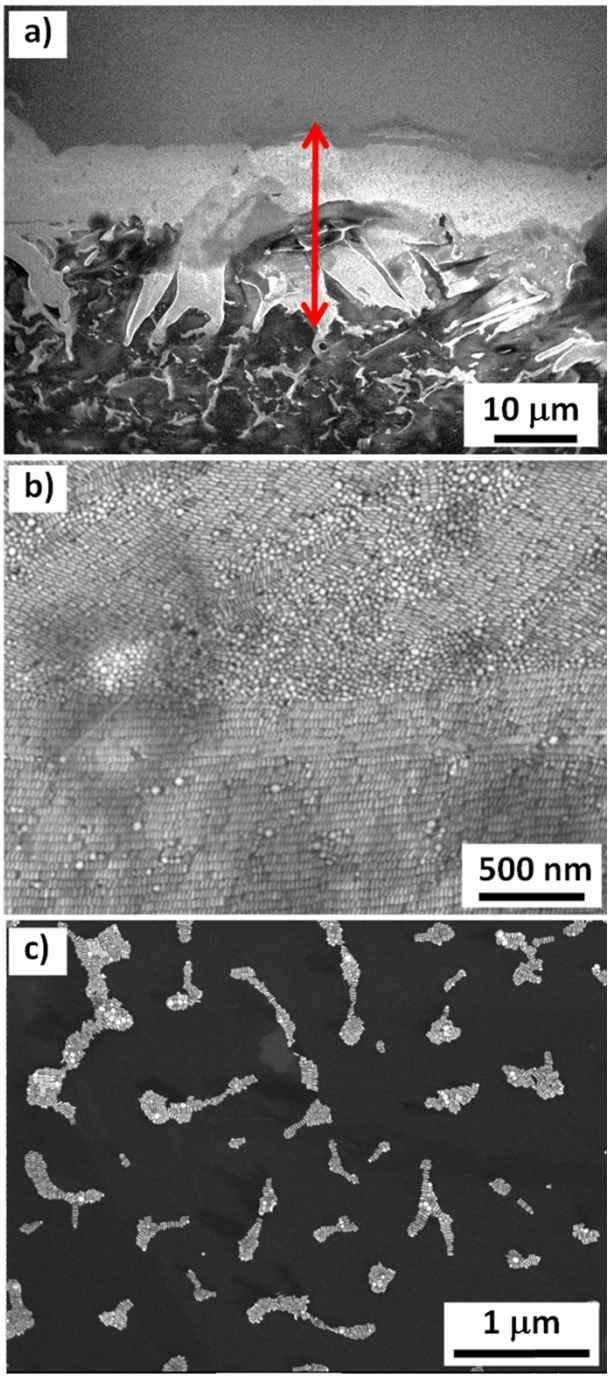

Figure SI6. a) Low magnification SEM image of Au nanorod (AR = 3.6) superstructures formed by aqueous droplet deposition on SiO_2 substrates. The arrow indicates the width of the area where nanorods are assembled; b) High magnification SEM image of assembled nanorods close to the edge; c) SEM image of small size assemblies formed in the center of the droplet.

The use of chlorobenzene was fundamental to obtain the long range ordering observed in our superstructures. Analogous droplet deposition of nanorod aqueous solutions

produced mixed parallel and perpendicular multilayered superstructures. Assemblies formed following a coffee stain mechanism in the explored nanorod concentration range (0.1 nM - 10 nM). Figure SI6 shows low and high magnification SEM images of parallel assemblies formed by evaporation of a 10 μL droplet of 2 nM aqueous Au nanorod solution. Nanorods were assembled in ordered structures only in the outer edge of the drop in a ring of 10 – 100 μm width, depending on the concentration of deposited solution. Very low density nanorod assemblies were found in the center of the drop, as shown in Figure SI6, c.

Droplet evaporation process

In order to elucidate the mechanism of nanorod superstructure formation optical images of the droplet during evaporation were acquired. The evaporation process is schematically described in Figure SI7a. Figures SI 6b-g show crossed polarized optical images taken at increasing times after the nanorod droplet deposition on the glass surface. In order to reproduce a slow evaporation rate, a 20 μL nanorod droplet was enclosed into an evaporation chamber and the microscope illumination source was directed away from the sample when measurements were not taken. Figure SI7b shows that a highly birefringent deposit started forming as the solvent evaporated ca. 60 min after droplet deposition. The width of this deposit increased inwards as a function of time as shown in Figure SI7b-f. The deposit was formed by domains (3-4 μm in diameter) that appear to form and accumulate at the edge of the drop. The domain birefringence indicated the formation of a liquid crystal phase driven by phase separation induced by drying and densification processes. According to the coffee stain effect, the bright birefringent ring width should increase with time until complete evaporation of the drop. However, from t_0 + 80 min we observed a suppression of the coffee stain mechanism resulting in movement of domain material towards the center of the drop (Figure SI7f). We speculate that this was due to the adhesion of formed domains to the air-solvent interface before they reached the contact line. As domains grew in size, they produced a surface viscosity that was much larger than the bulk viscosity, facilitating nanorod resistance to radially outward flow. As a result, the drop edge depinned and started moving inward. At the end of the process, when the droplet completed dried, a thin ring of aligned nanorods was found at the edge of the drop whereas the majority of nanorod domains settled in the core of the droplet (Figure SI7g).

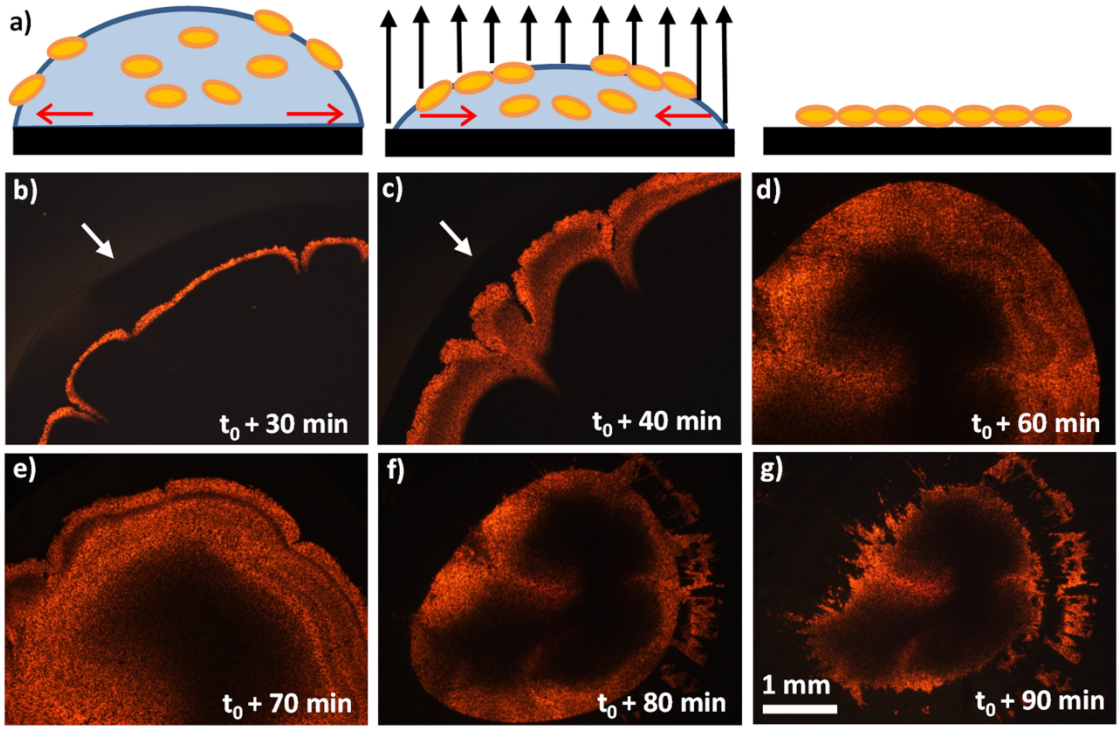

Figure SI7. a) Schematic of droplet-evaporation induced formation of Au nanorod parallel superstructures; b-g) optical images of Au nanorod droplet deposited on glass

cover slip during evaporation under crossed polarizers. The edge of the drop is indicated by the white arrow in b –c). Illumination is from above. Scale bar for all optical images is 1 mm.

Droplet evaporation/stamping method

Parallel Au nanorod superstructures were formed following a method illustrated in Scheme SI1a,b. The fabrication process comprised two steps: a) evaporation of a nanorod droplet solution on a support and b) stamping of the resulting nanorod array on a receiving support. Specifically, a drop (scheme 1a.1) of Au nanorod chlorobenzene solution was deposited on a SiO_2 support and left to evaporate under controlled conditions (T = 20 ºC, Humidity = 70%, evaporation time = 3 h). As solvent evaporated, nanorods assembled into monolayer islands that gradually grew up in size and moved to the interface between solvent and air (a.2). Upon solvent evaporation, nanorods assembled on the support. Arrays with a high degree of order were already obtained at this stage (data not shown) but the concomitant deposition of excess surfactants (a.3) prevented their use for SERS analysis, since nanorod arrays detached from the SiO_2 support when immersed in analyte solutions. In order to improve adhesion of arrays to the support and clean off residual organic matter an additional stamping process was introduced, as shown in scheme 1b. Specifically, a receiving support (glass coverslip) was pressed on the original SiO_2 support containing the arrays for 30 s (scheme 1b.1). Nanorods transferred intact on the glass support along with the residual organic matter (b.2), which was eliminated by immersion in isopropanol, followed by multiple rinses with clean isopropanol (b.3).

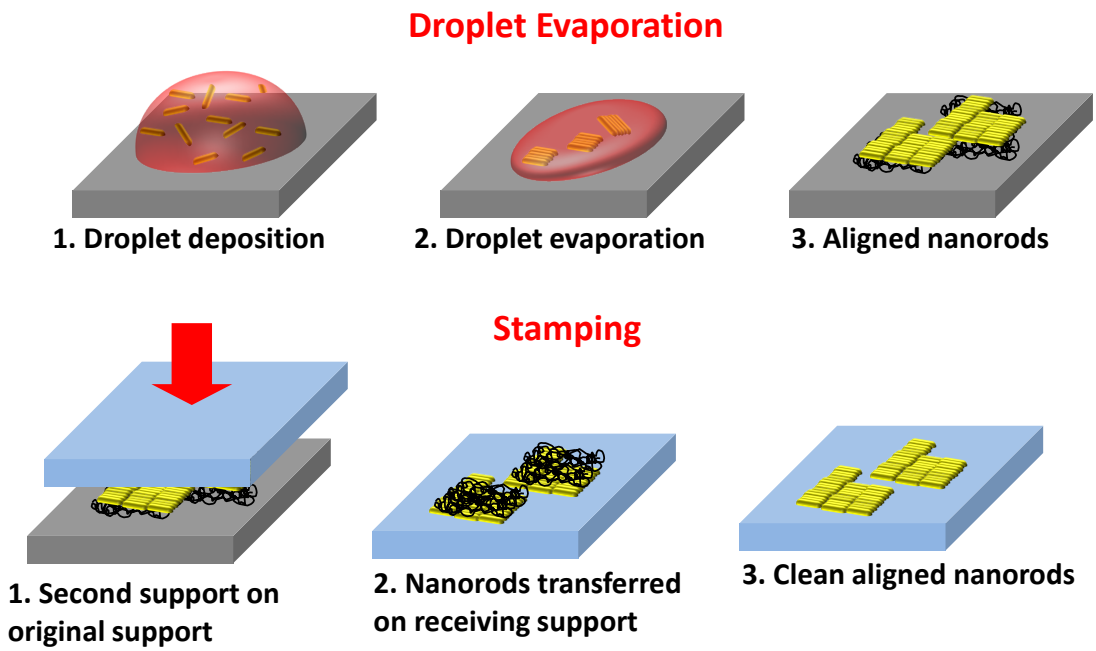

Scheme SI1. Formation of parallel superstructures by combined droplet evaporation/stamping technique; a1-3) droplet deposition and droplet evaporation process; b1-3) stamping and cleaning of nanorod arrays on glass support.

Simulations

Figure SI8 shows extinction, absorption and scattering spectra of an individual 11×40 nm nanorod with excitation polarized perpendicular (a) and parallel (b) to the nanorod long axis. Maxima were found at 511 nm and 733 nm. Extinction, absorption and scattering spectra of nanorods 11×40 nm arranged into 2×6 arrays with internanorod distance of 2.5 nm with excitation polarized perpendicular (c) and parallel (d) to the nanorod long axes. Maxima were found at 540 nm and 720 nm. Simulations were run by solving the Maxwell's equations using a boundary element method with MNPBEM Matlab toolbox.

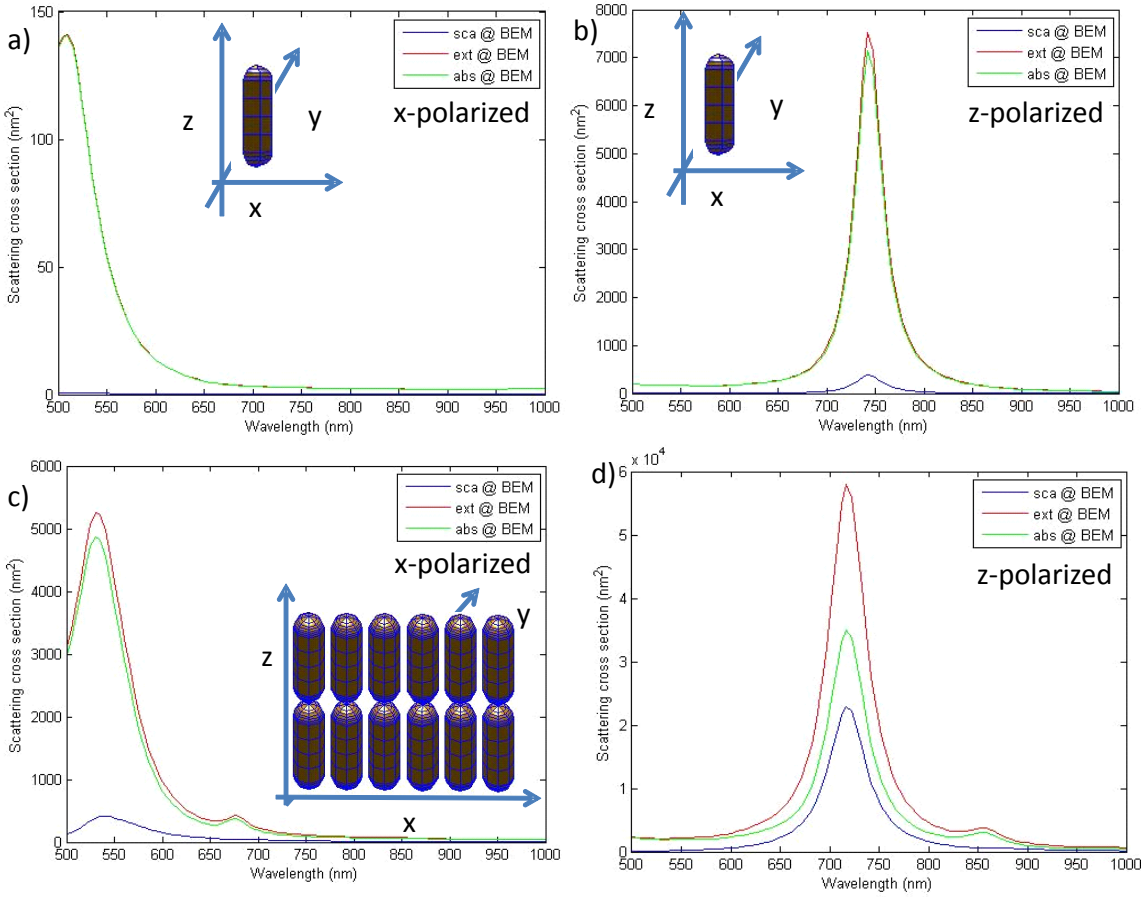

Figure SI8. Calculated extinction, scattering and absorption spectra for a, b) individual 11x40 nm nanorods for incident light polarized along x and z direction; c,d) nanorods parallel 11x40 nm assembled into a 2×6 array with internanorod distance of 2.5 nm for incident light polarized x and z direction.

Correlated polarized optical microscopy/electron microscopy

Correlated optical/electron microscopy imaging revealed that the optical features of superstructure domains were highly dependent on the degree of nanorod internal packing. For example color transition from red to pale green was observed in domains where nanorods were only loosely packed into side-by-side configuration, see Figure SI8. The colors were correlated to selective excitation of the longitudinal and transversal surface plasmon resonance (SPR) modes of the nanorods, respectively.

A corresponding transition from 735 nm to 580 nm was observed in the spectra recorded under polarized light oriented parallel and perpendicular to the nanorod long axes. A correlated SEM image of the optically characterized nanorod domain is shown as inset in Figure SI8b, confirming the high degree of order but lose packing of the nanorods in the imaged area.

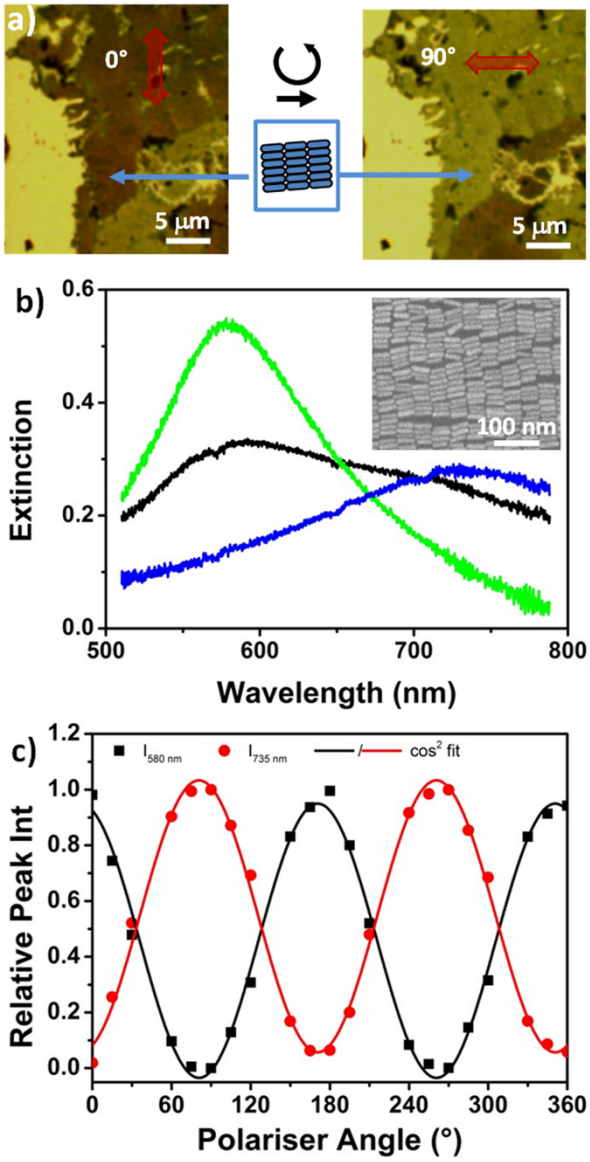

Figure SI9. a) Polarized transmission images of Au nanorod domains showing red to pale green color transition associated to the relative orientation of polarized light with the long axes of nanorods that constitute the domains; b) Extinction spectra of the nanorod domain indicated in a) acquired with nonpolarized excitation (black) and with polarized excitation perpendicular (0°, green curve) and parallel (90°, blue curve) to the nanorod longitudinal axes. Inset: SEM image showing the ordering of the nanorods within the domain where the spectra were taken; c) Relative contributions of the transversal (black) and longitudinal (red) mode to the overall extinction spectrum dependent on the polarizer angle with least-squares $\cos^2 \theta$ fit.

Figure SI9c shows the relative contribution of the transversal (black) and longitudinal (red) plasmon extinction to the overall extinction spectra as function of the polarization angle. A $\cos^2$ curve fit to these data indicates a reproducible polarization-dependent behavior of nanorod domain extinction intensity. The low intensity measured perpendicularly to the domain long axis corresponded to a max intensity along the direction of the domain long axis, indicating an almost perfect alignment of individual nanorods within the domain.

QR code generation and decoding

Figure SI10 shows a schematic of the encoding and verification process. From an optical image (center of the diagram) of the unique nanorod domain pattern recorded under polarized illumination a histogram of the green values was obtained using image processing software like Image J. To encode this for each area unique data we concentrated on a fixed range of green values from 60 to 159, the most relevant region of the full range (0 to 255), where the largest difference between samples was observed. The y-axis values were converted into a continuous string of 200 characters, which in turn were converted into a QR code with readily available software (e.g. http://qrcodemakr.com). As verification tool, the process was reversed. A scanned image of the QR code was de-codified by an online QR code reader (e.g. http://online-barcode-reader.inliteresearch.com) producing a string of 200 characters. The number string could be converted back into the original histogram with a matlab code containing all relevant decoding information.

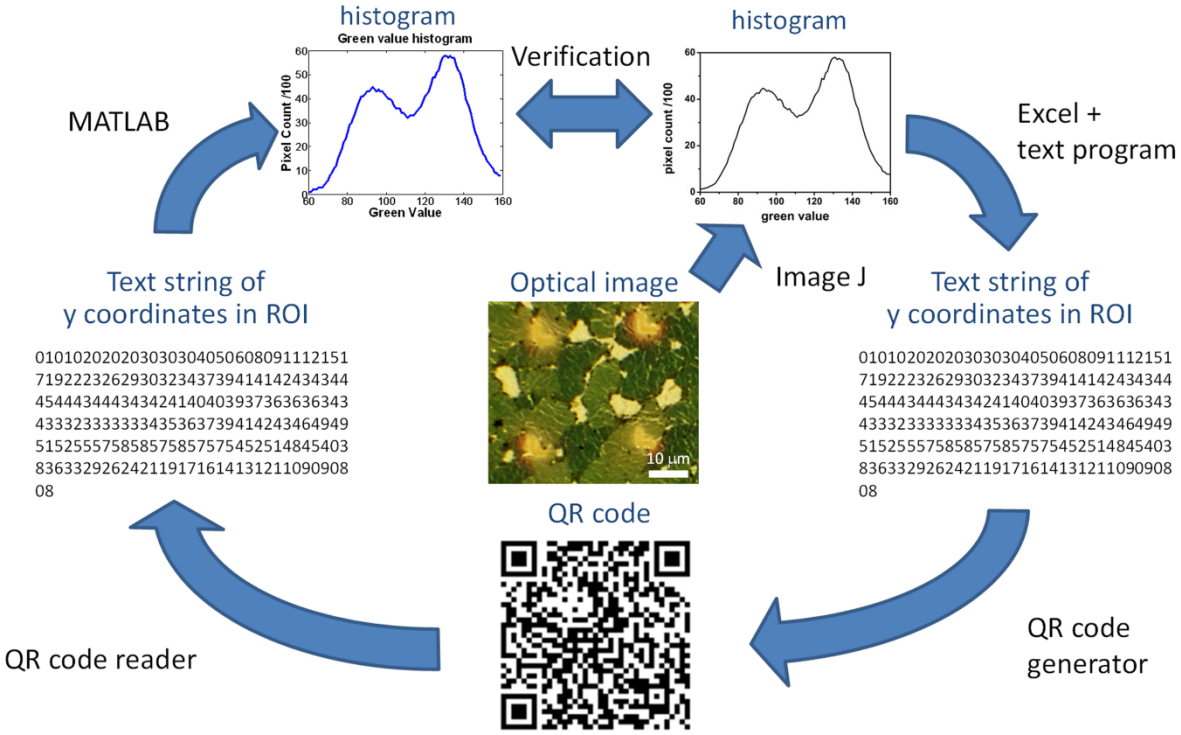

Figure SI10. Scheme of the process describing the generation of a unique text string (and corresponding QR code) from a polarized transmission optical image of Au nanorod domains (encoding). The Corresponding decoding process is also described.

Details of MATLAB Code:

```
clear all;
disp('load file');
[image_id, image_pathname, filterindex] = uigetfile;
image_path_full = strcat(image_pathname, image_id);

fid = fopen(image_path_full);
QRCODENUMBER = fgets(fid);
```

```
fclose(fid)

MatrixQR = zeros(100, 2);

row = 1;
yFirstDigit = 1;
yNumberDigits = 2;
for x = 60:159
Packet = QRCODENUMBER(yFirstDigit:yNumberDigits);
Temp1 = str2double(Packet);

MatrixQR(row,1) = x;
MatrixQR(row,2) = (Temp1);
yFirstDigit = yFirstDigit + 2;
yNumberDigits = yNumberDigits + 2;
row = row + 1;
end

plot(MatrixQR(:,1),MatrixQR(:,2));
title('Green value histogram');
xlabel('Green Value');
ylabel('Pixel Count /100');
```